Interfacial stability, oxidation response and mechanical properties of a Nicalon™ Fibre reinforced chemical bonded ceramic matrix composite

A. BANDYOPADHYAY, P. B. ASWATH
Department of Mechanical and Aerospace Engineering and Materials Science and Engineering Program, University of Texas at Arlington, Arlington, TX 76019, USA

A slurry of monoaluminum phosphate with fine Al_2O_3 powder was infiltrated into eight harness satin fabric of Nicalon™ fibres. The infiltrated fabrics were laid up in 16 plies and then cured in an autoclave. Due to the chemical reaction between alumina and monoaluminum phosphate, aluminum phosphate was produced. Carbon coated and uncoated fibres were used to manufacture these composites to produce weak and strong interfaces between matrix and fibres. Two different processing routes were used during manufacturing, which resulted in different amounts of porosity content in the final composites. Thermogravimetric analysis carried out at 850 °C for 6000 min in air showed negligible weight change, indicating stable fibres in the composites. Four-point bend flexure tests were conducted at room temperature, 700 and 850 °C. Strong interface composites completely failed at high temperatures due to fibre fracture, but a shear dominated delamination-type interface failure was observed for the weak interface composites. Strong interface composites exhibited better flexure strengths than the weak interface composites under all conditions of processing and orientations. However, the weak interface composites absorbed significantly larger amounts of energy before failure compared to the strong interface composites. Little influence of porosity content was seen on flexure properties both at room and elevated temperatures. High temperature failure behaviour is explained using classical lamination theory.

1. Introduction

Despite their high strength to weight ratio, good thermal stability, high wear resistance, high hardness and high corrosion resistance, the use of ceramic materials in structural applications is hindered by their inherent brittleness. Extensive research work is currently underway to improve the toughness of the ceramic materials [1-5]. Some of the common approaches are design of microstructures which promote crack bridging, crack branching and microcrack toughening, consequently expending energy during crack propagation [5-10]. To implement these toughening mechanisms into the final material a number of innovative processing techniques, like slurry infiltration, hot-pressing, hot isostatic-pressing, reaction bonding, sol–gel processing, etc., have been used over the past few decades. The most common requirement for all of the above mentioned processes is consolidation at high temperature and high pressure. During fabrication of continuous fibre reinforced composites these high temperature processes may cause mechanical and chemical degradation of fibres and of the fibre matrix interface. Chemical bonded ceramic composites offer an attractive alternative [11-15]. This

process is similar to that of the thermosetting polymer matrix composite fabrication technique where composites are fabricated by *in situ* chemical reaction in the matrix material. As a result this process eliminates the high temperature and high pressure consolidation step. This process is inexpensive with a smaller chance of fibre degradation. In addition, due to low matrix shrinkage during curing, it is also useful in near net-shape manufacturing [15].

Instead of using the traditional continuous fibre composite approach, an eight harness satin weave of Nicalon™ fabric was used as the reinforcement and aluminum phosphate used as the matrix material. The use of fabric for reinforcement has gained increasing technological interest over the past decade. Fabric reinforced composites provide more balanced properties in the fabric plane and a better impact resistance due to the bidirectional reinforcement [16-19]. It has also been established that a composite with a strong matrix/fibre bond has a higher strength but lower toughness [5]. In order to evaluate the effect of the fibre/matrix interface on flexure properties a weak and a strong interface were chosen. Carbon coated Nicalon™ fibres were used to produce a weak inter-
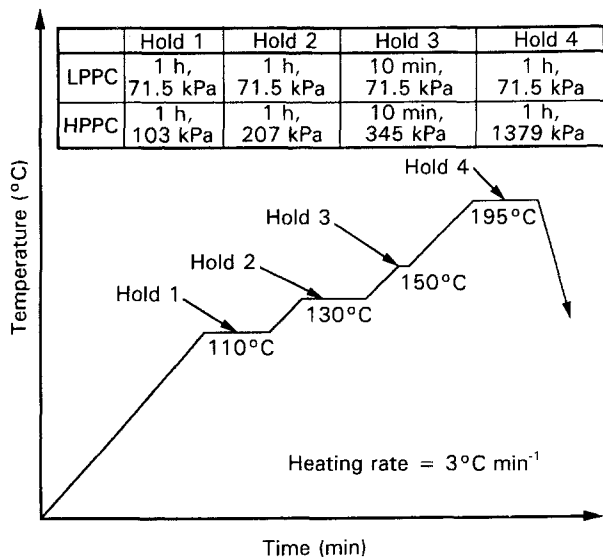
	Hold 1	Hold 2	Hold 3	Hold 4
LPPC	1 h, 71.5 kPa	1 h, 71.5 kPa	10 min, 71.5 kPa	1 h, 71.5 kPa
HPPC	1 h, 103 kPa	1 h, 207 kPa	10 min, 345 kPa	1 h, 1379 kPa

Temperature (°C)

Hold 4

Hold 3   195°C

Hold 2   150°C

Hold 1   130°C

110°C

Heating rate = 3°C min⁻¹

Time (min)

Figure 1 Schematic representation of processing routes of the low and high pressure processed composites.

face, while uncoated Nicalon™ fibres were used to promote a strong interface by the formation of a bond between the matrix and the fibres.

In the present work, thermal stability of the composites were tested by thermo-gravimetric analysis at 850 °C for 6000 min. Four-point bend flexure tests were conducted at room temperature, 700 and 850 °C to study the effect of several variables, which included the type of interface, porosity content and orientation of the ply. A shear dominated delamination type failure occurred between the loading pin and support pin in the weak interface composites. For strong interface composites, a clear fracture within the even moment zone was observed during high temperature testing. An analysis of the residual stress build-up due to coefficient of thermal expansion (CTE) mismatch between fibre and matrix, was done using classical lamination theory.

2. Processing and experimental techniques

The ceramic matrix composites were processed at Aloca Technical Lab., PA, 10–20 μm diameter Nicalon™ fibres were used to manufacture eight harness satin weave fabric as a fibre reinforcement. The typical composition of these amorphous SiC fibres were 59 wt % Si, 31 wt% C and 10 wt % O. Because of the fibre degradation and the possibility of cracking due to shrinkage, high temperature consolidation techniques could not be used for these materials. A chemical bonding processing technique which could be carried out at low temperatures was used as an alternative. A slurry was made using 50 vol fraction of fine alumina powder in a solvent of 50 vol fraction of monoaluminum phosphate. Sheets of slurry infiltrated fabric laid up in 16 plies in an autoclave were consolidated using two processing routes. One route used a constant pressure of 71.5 kPa during the temperature ramping cycle, while the other process employed an increasing pressure step (from 104 to 1379 kPa) during

every hold period of the cycle. The composite processed by the former route is referred to as the "low pressure processed composite" (LPPC) while the latter is referred to as the "high pressure processed composite" (HPPC). The processing routes are shown schematically in Fig. 1. The LPPC had a significantly larger porosity content than the HPPC. During curing, chemical reaction took place between mono-aluminum phosphate and alumina, forming aluminum phosphate [20]. This helped to form good bonding between the matrix and the reinforcement. Two types of SiC fibres were used to manufacture these composites, one was coated with carbon and the other left uncoated. The presence of a carbon coating on the fibre protected it from chemical attack from the matrix and helped to form a weak bond with the matrix. On the contrary, in the composites made with uncoated fibres, the matrix could attack the fibres and produce strong bonds between the fibre and the matrix.

A Perkin-Elmer series 7000 thermogravimetric analyzer was used to perform high temperature isothermal oxidation experiments. Specimens of known initial weight and cross-sectional area were exposed for 6000 min at 850 °C in normal air environment at a pressure of 1.013×10^5 Pa. The change in weight was monitored continuously using a data acquisition system. Thermal degradation of the fibre and the matrix material was studied using a Camica Camibax electron probe microanalyser. Four-point bend specimens, $50 \times 10.3 \times 5 \, mm^3$, were machined from a large square block of composite panel, $228.5 \times 228.5 \times 5 \, mm^3$ in size. Room and high temperature flexure tests were carried out using a servo hydraulic testing machine, Instron 1331, at a constant stroke rate of $12.7 \, mm \, min^{-1}$. High temperature flexure tests at 700 and 850 °C were carried out in an ATS high temperature split furnace with a 10 cm uniform heating zone. Once the temperature was reached, a 15 min soaking time was provided before testing. Fractographic analyses were carried out using a Cambridge Stereoscan 120 scanning electron microscope (SEM).

3. Results
3.1. Physical properties
Table I shows the physical properties of the different composites. In the HPPC the % void fraction of the material was significantly lower than in the LPPC, with a consequential increase in density. In addition, the composites with a strong fibre/matrix interface showed low amounts of void content compared to the weak interface composites. This can be attributed to the fibre/matrix interaction which promoted the spread of the matrix to all the regions of the composite.

3.2. Thermal stability
It has been reported [15] that at higher temperatures (> 1000 °C) aluminum phosphate can decompose into alumina and phosphorous pentoxide by the reaction

$$2AlPO_4 \longrightarrow Al_2O_3 + P_2O_5$$

TABLE I Physical properties of the composites

Processing	Interface type	Orientation	Porosity (%)	Density (g cm^{-3})	Test temperature
LPPC	Strong	(0/90) (+ 45/ − 45)	25.0	1.93	RT^a, 700 °C, 850 °C
	Weak	(0/90) (+ 45/ − 45)	28.0	1.86	RT^a, 700 °C, 850 °C
HPPC	Strong	(0/90) (+ 45/ − 45)	10.0	2.31	RT^a, 700 °C, 850 °C
	Weak	(0/90)	15.0	2.25	RT^a, 700 °C, 850 °C

^{a} RT = room temperature.

In addition the decomposition of the coating can occur by a reaction of the type

$$2C + O_2 \longrightarrow 2CO_2$$

and oxidation of the fibres can occur by a reaction of the type

$$2SiC + 4O_2 \longrightarrow 2SiO_2 + 2CO_2$$
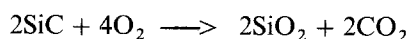
Thermogravimetric analyses were carried out for LPPCs and HPPCs with both the strong and weak fibre/matrix interfaces at 850 °C in a normal air environment at a pressure of 1.013×10^5 Pa. Fig. 2a shows the normalized weight gain (weight gain/original weight) of the sample as a function of time for the weak interface type composites. Fig. 2b shows the same for the strong interface type composites. It is important to note that even after 6000 min at 850 °C the total weight gain was less than 1% of the initial weight, indicating that there was negligible change occurring. The only difference between the strong and weak interface composites was that in the former there was a gradual increase in weight, which saturated after 3000 min. In the case of the weak interface composites, after an initial rapid increase in weight up to 500 min the weight gain saturated. No evidence of weight loss due to carbon sublimation was observed in any of the composites. This measurement, albeit sensitive, does not provide a true understanding of the interactions at the microscale at the fibre/matrix interface. It is interesting to note that porosity content did not play a role in the rates of oxidation, with HPPC and LPPC exhibiting about the same rates of oxidation. This is contrary to the belief that interconnected internal porosity is detrimental to oxidation behaviour. This indicates that at 850 °C little or no oxidation of the fibres, matrix or the coating was taking place.

Extensive electron microprobe analysis with elemental dot mapping was conducted on as-received and oxidized samples to study the fibre degradation and element migration. No significant fibre and matrix degradation was observed up to a magnification of × 2000. As the weight gain was insignificant, very little fibre degradation was expected. Si, Al and P X-ray dot maps were similar for the as-received and
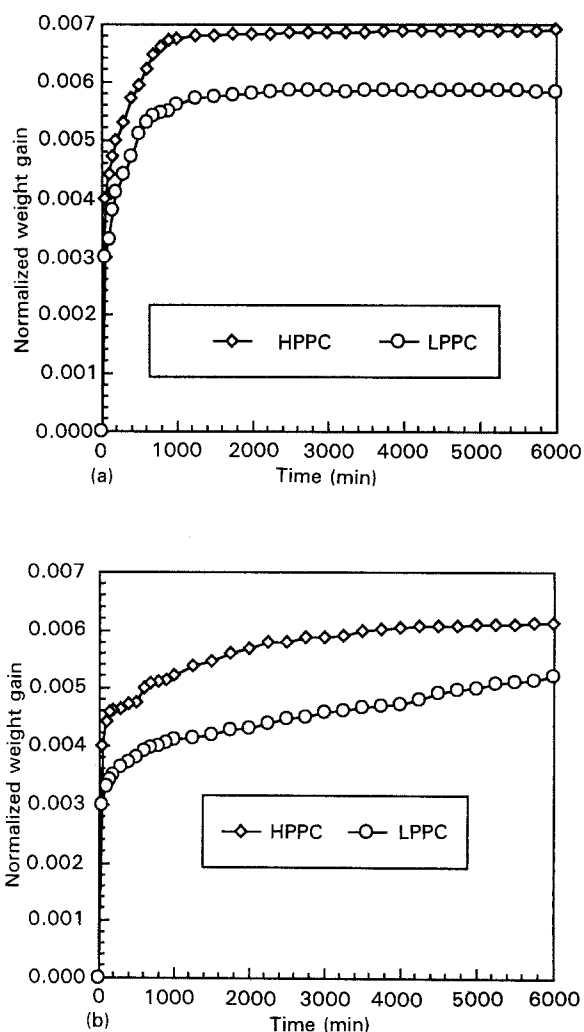

Figure 2 (a) Normalized weight change as a function of time at 850 °C for weak interface composites. (b) Normalized weight gain as a function of time at 850 °C for the case of strong interface composites.

oxidized samples. Fig. 3a shows the scanning electron micrograph of the HPPC with a weak interface after 6000 min exposure at 850 °C. Fig. 3b and c show the Al and Si X-ray dot map of the same region, respectively. A clean fibre surface without any degradation can be observed. A similar type of behaviour was observed in the oxidation of the other composites.
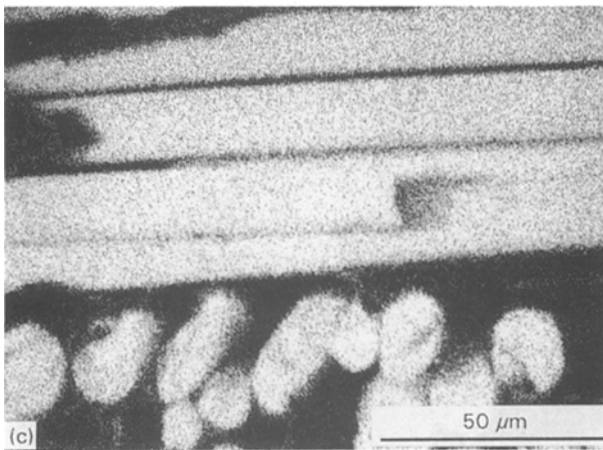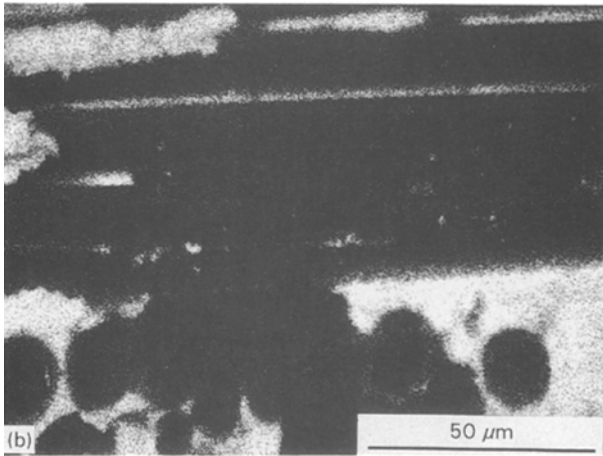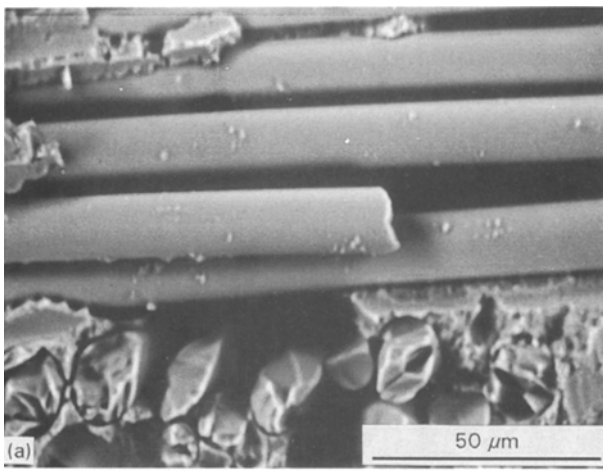
4207

Figure 3 (a) SEM micrograph of the HPPC, weak interface; (b) X-ray dot map showing Al and (c) Si distribution

classical analysis of the residual stress developed due to CTE mismatch between the fibres and the matrix.

The experimental results will be discussed in two major groups which include: (a) low pressure processed composites (LPPC), presented in Section 3.3.3 and (b) high pressure processed composites (HPPC) presented in Section 3.3.4. The primary differences in these two classifications is in the porosity content of the composites. Within each of these groups the role played by: (i) orientation of the ply; (ii) type of the fibre/matrix interface, and (iii) temperature of flexure testing will be discussed. Section 3.3.5 examines the change in the modulus of elasticity in bending for different types of composites.

In the overall context, composites with a weak interface were more damage tolerant than the composites with a strong interface. This is a consequence of the greater amount of shear stress dominated delamination in composites with a weak fibre/matrix interface as compared to fibre breakage-type failure in the strong interface composites.

3.3.1. Two-dimensional finite element model to represent the stress state in a flexure bar

A simple two-dimensional finite element model was used to obtain the stress distribution in a bar under four-point bend loading. The material modelled was an isotropic monolithic material, to enable a physical understanding of the stress distributions to be obtained. The mesh generation and analysis was done using the FEM code ALVIN. Only one-half of the flexure bar was modelled due to symmetry. Triangular elements were used with 92 nodal points. Fig. 4a shows the finite element model used. A point load was
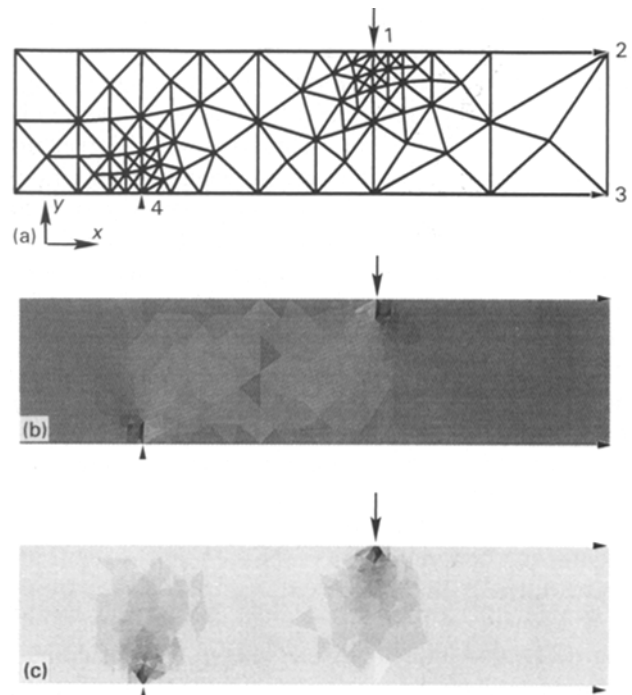
3.3. Room and high temperature flexure tests

To gain a better understanding of the mechanism of failure a knowledge of the stress state within the four-point bend flexure bar was required. A simple two-dimensional finite element model was developed to determine the values of normalized stresses at different regions of the flexure bar – Section 3.3.1 details the simulations done. At elevated temperatures the difference in CTE of the fibres and matrix could result in significant amounts of residual stress within the composite, weakening it. Section 3.3.2 presents a simple

Figure 4 (a) Finite element model with loading point and constraints. (b) Shear stress (τ_{xy}) distribution. (c) σ_{yy} distribution.
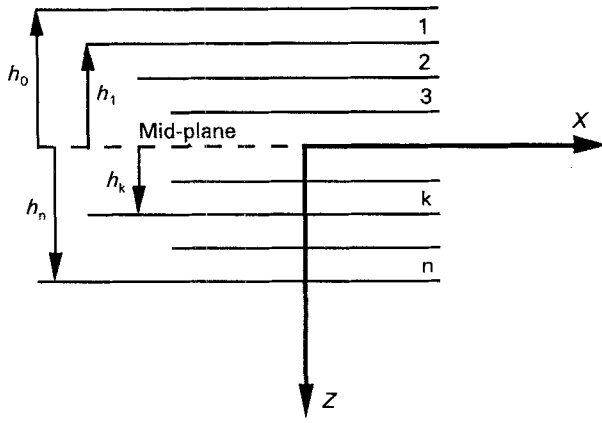
Figure 5 Geometry of the composite laminate model.

applied at point 1 and constraints were placed at points 2 and 3 to prevent motion in the x-direction. Point 4 was constrained from movement in the y-direction but was free to move in x-direction. Remeshing was continued until the error was below 6%. Fig. 4b shows the τ_{xy} and Fig. 4c shows σ_{yy} distributions in the flexure bars. The shear stress was at a maximum in the region between load point 1 and support point 4, and reached numerical values as high as 45 times the point load. The σ_{yy} plot shows that large stresses developed in the flexure bar near the point of load and support.

3.3.2. Analysis of residual stress due to coefficient of thermal expansion mismatch between the fibres and the matrix

A change in temperature could cause changes in the dimension of fibre reinforced composites which are a function of the temperature change and the initial dimension of the sample. Fig. 5 is a schematic diagram of the material model used. Lamina strain ε_j of any lamina can be calculated from the laminate midplane strains and plate curvature by:

$$\varepsilon_j = \varepsilon_j^0 + z\kappa_j \qquad (1)$$

where ε_j^0 is the midplane strain, κ_j is the midplane curvature and z is the distance from the midplane. Typically the change in thermal strain, ε^T (from free expansion of lamina without constraint), is given by:

$$\varepsilon^T = \alpha\Delta T \qquad (2)$$

where α is the coefficient of thermal expansion and ΔT is the change in temperature. It is well established that thermal strains do not produce a resultant force or moment when the body is completely free to expand, bend or twist. However, each of the individual lamina in a laminate is not completely free to deform, its deformation is influenced by other laminae. The stress in the laminae are produced by the strains that are in excess of the thermal strains for free expansions. When there are no external stresses, the strains that cause stress due to temperature change can be referred to as

mechanical strains, ε_j^M, and are given by:

$$\varepsilon_j^M = \varepsilon_j - \varepsilon_j^T \qquad (3)$$

where ε_j^T is the thermal strain from free expansion. The generalized Hookean law that relates stress and strain is given by:

$$\sigma_i = Q_{ij}\varepsilon_j \qquad (4)$$

where Q_{ij} is the stiffness matrix, σ_i is the stress component and ε_j is the strain component. When an external load is applied, the total stress in the lamina, σ_i, is given by:

$$\sigma_i = \sigma_i^T + \sigma_i^{Ex} \qquad (5)$$

where σ_i^T is the stress due to ε_j^M and σ_i^{Ex} is the stress due to external applied load. From Jones's [21] analysis of classical laminated plate theory, the total plate constitutive equation can be written as:

$$\begin{bmatrix} N_i \\ \hline M_i \end{bmatrix} = \begin{bmatrix} A_{ij} & B_{ij} \\ \hline B_{ij} & D_{ij} \end{bmatrix}\begin{bmatrix} \varepsilon_j^0 \\ \hline \kappa_j \end{bmatrix}$$

or,

$$\begin{bmatrix} \varepsilon_j^0 \\ \hline \kappa_j \end{bmatrix} = \begin{bmatrix} a_{ij} & b_{ij} \\ \hline b_{ij} & d_{ij} \end{bmatrix}\begin{bmatrix} N_i \\ \hline M_i \end{bmatrix} \qquad (6)$$

where,

$$A_{ij} = \sum_{k=1}^{n} (\overline{Q_{ij}})_k (h_k - h_{k-1})$$

$$B_{ij} = \tfrac{1}{2}\sum_{k=1}^{n} (\overline{Q_{ij}})_k (h_k^2 - h_{k-1}^2) \qquad (7)$$

$$D_{ij} = \tfrac{1}{3}\sum_{k=1}^{n} (\overline{Q_{ij}})_k (h_k^3 - h_{k-1}^3)$$

and

$$\begin{bmatrix} a_{ij} & b_{ij} \\ b_{ij}^T & d_{ij} \end{bmatrix} = \begin{bmatrix} A_{ij} & B_{ij} \\ \hline B_{ij} & D_{ij} \end{bmatrix}^{-1}$$

where $(\overline{Q_{ij}})_k$ is the stiffness matrix for the generally orthotropic lamina, A_{ij} is the extensional stiffness, B_{ij} is the coupling stiffness, D_{ij} is the bending stiffness, N_i is the force resultant, M_i is the moment resultant, n is the total number of plies, ε^0 is the midplane strain and κ is the midplane curvature. From Fig. 5, it can be seen that h_k is the distance between the midplane and the kth lamina and similarly $h_{(k-1)}$ is the distance between the midplane and $(k - 1)$th lamina. ε_j^M is given by:

$$\varepsilon_j^M = a_{ij}N_i + b_{ij}M_i - (a_{ij}N_i^T + b_{ij}M_i^T) \qquad (8)$$

where N_i^T is the residual thermal stress resultant and M_i^T is the residual moment resultant and is given by:

$$[N_i^T] = \Delta T \sum_{k=1}^{n} (\overline{Q_{ij}})_k (\alpha)_k (h_k - h_{k-1})$$

and

$$[M_i^T] = \Delta T \sum_{k=1}^{n} (\overline{Q_{ij}})_k (\alpha)_k (h_k^2 - h_{k-1}^2) \qquad (9)$$

where ΔT is the temperature difference and α is the coefficient of thermal expansion. For the case of eight harness satin weave fabric, assuming uniform average
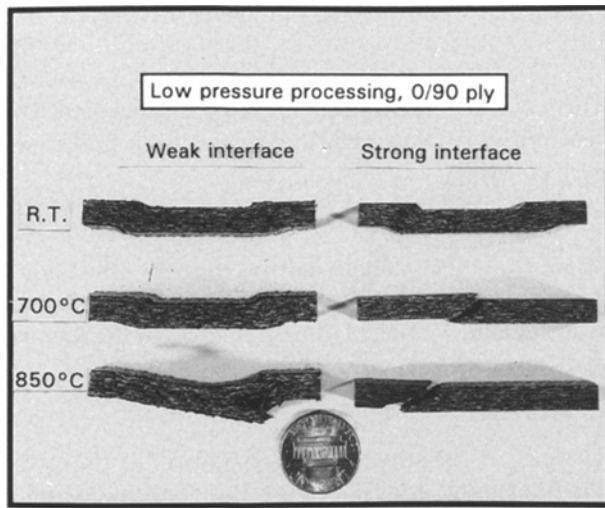
Figure 6 A low magnification photograph of (0/90)_{4s}-type LPPC tested at different temperatures showing different types of failures under four-point bend loading.
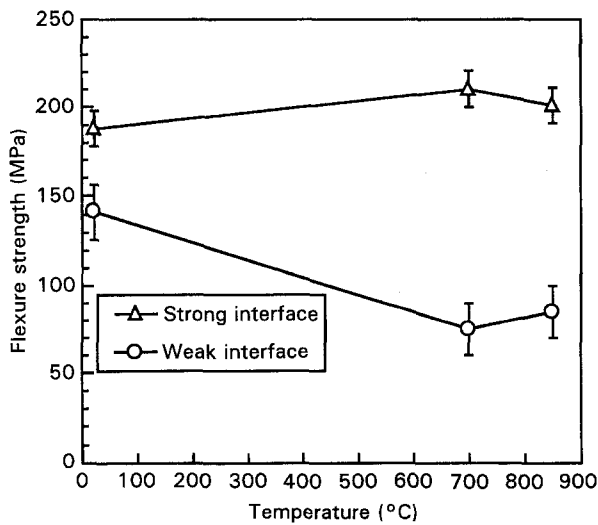

Figure 7 Flexure strength of low pressure processed (0/90)_{4s}-type weak and strong interface composites tested at three different temperatures.

midplane strain and curvature, A_{ij}, B_{ij} and D_{ij} can be replaced by [22]:

$$\overline{A_{ij}} = 0.35[1.83\,A_{ij} + \overline{A_{ij}^u}]$$

$$\overline{B_{ij}} = 0.64\,B_{ij} \qquad (10)$$

$$\overline{D_{ij}} = 0.35[1.83\,D_{ij} + \overline{D_{ij}^u}]$$

where the $\overline{A_{ij}^u}$ and $\overline{D_{ij}^u}$ are the modified extensional and bending matrices for the undulated portion in the fabric, respectively; A_{ij} and D_{ij} are the regular extensional and bending matrices for straight fibre portion of the fabric, respectively.

For a fixed constraint, with increasing temperature, ε_j^M will increase and result in a higher σ_i^T. Now, from Equation 5, it is clear that if failure occurs due to a constant total stress, then at higher temperatures (HT) requirements of the external applied stress would reduce due to an increase in the residual thermal stress contribution.
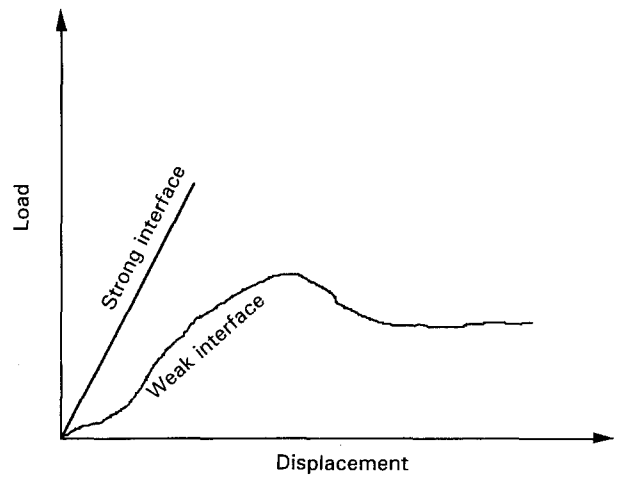

Figure 8 A typical load versus displacement curve for weak and strong interface composites.

3.3.3. Low pressure processed composites (LPPC)

Two-ply orientations of (0/90)_{4s} and (+ 45/ − 45)_{4s} were chosen and results will be discussed in terms of these two orientations.

3.3.3.1. (0/90)_{4s} ply orientation in LPPC. The variables used in this analysis included the type of fibre/matrix interface and temperature of testing. Fig. 6 shows a low magnification photograph of the different types of failure as a function of temperature. All the composites which had a weak fibre/matrix interface failed by shear induced delamination between the pins of the load span and the support span. Note that there was no break in the specimen and the test was stopped when there was a significant drop in the load supported by the specimen. The composites with a strong fibre/matrix interface failed by a clean break through the fibres and matrix at an elevated temperature, whilst at room temperature they also exhibited a delamination-type of failure. Fig. 7 shows the flexure strength of the composite for the (0/90)_{4s} orientation as a function of temperature. Fig. 8 is a diagram showing a schematic of the load versus displacement plots of the composites with weak and strong fibre/matrix interfaces. Note that despite having a lower flexure strength the composites with a weak fibre/matrix interface exhibited a much larger damage tolerance as compared to the composites with a strong fibre/matrix interface.

The flexure strengths in Fig. 7 indicate that after a drop in strength at 700 °C for the composite with the weak fibre/matrix interface the strength increased at 850 °C. This result indicates that up to 700 °C there was little fibre/matrix interaction and as the temperature was increased from room temperature to 700 °C, there was a drop in flexure strength. At 850 °C it was possible that the carbon coating on the Nicalon™ fibres were sufficiently degraded leading to a bond between the fibre and matrix. This led to the formation of an interface that was stronger than the one at room temperature and 700 °C, and a consequent increase in strength. In all the tested samples there were

4210

some ply failures about one-ply thick on the top and bottom plies at the point of contact with the load and support pin. The large normal stresses at the point of contact of the pins promoted the failure of the plies.

In the composite with a strong fibre/matrix interface tested at room temperature a delamination-type failure occurred, in a fashion similar to that observed in the composites with the weak fibre/matrix interface, shown in Fig. 6. The reason for the delamination-type failure at room temperature can be attributed to the large amounts of porosity present. The porosity enabled fibre sliding to occur, even with a strong fibre/matrix interface, leading to a delamination-type failure. However, as shown in Fig. 6, at elevated temperatures complete fibre and matrix breakage was the cause of failure. The angle of failure was 45° to the loading direction, consistent with the mode of failure for the $(0/90)_{4s}$ orientation. Failure initiated on the tensile side of the constant moment region and rapid fracture occurred with little energy absorbed.

It is important to note that at elevated temperatures the flexure strength is a synergistic interaction of at least three variables which include: (i) change in the fibre/matrix interface; (ii) change in the fibre properties; and (iii) residual stress developed due to CTE mismatch between the fibre and the matrix. The initial small increase in flexure strength in the composite with the strong interface can be attributed to the change in mechanism of failure from delamination-type failure at room temperature to fibre breakage at 700 °C. At 850 °C the decrease in flexure strength can be attributed to the degradation of fibre and/or matrix, as well as their interfaces, with an increase in temperature. In addition, stresses arising from CTE mismatch between the fibre and the matrix could lead to a deterioration of the flexure properties. This result was analytically derived in an earlier section to prove the point. It is important to note that despite the drop in strength at 850 °C in the composite with the strong interface, it is still stronger than the weak interface composite at 850 °C. This indicates that despite the degradation in properties due to an increase in temperature, the presence of a strong interface yields a higher strength than a weak interface.

Fig. 9 is a scanning electron micrograph of the fracture surface of an LPPC with a strong fibre/matrix interface tested at 850 °C. Large pores were present and the primary mode of failure appeared to be due to fibre and matrix failure with very little fibre pull-out. The plane of fracture was at an angle of 45° to the loading axis.

3.3.3.2. (+45/−45) ply orientation in LPPC. Fig. 10 shows a low magnification photograph of the deformed and failed specimens of the $(+45/−45)_{4s}$ oriented LPPC with weak and strong fibre/matrix interfaces. As in the $(0/90)_{4s}$ case, deformation/delamination-type failure occurred for specimens with a weak fibre/matrix interface, while specimens with a strong fibre/matrix interface failed by fibre and matrix cracking (except at room temperature where the strong interface composite failed by a delamination-type of failure due to the large porosity content). The
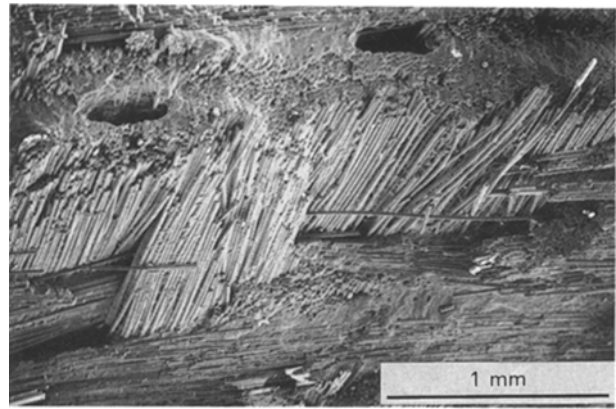
Figure 9 SEM fractograph of the low pressure processed strong interface composite tested at 850 °C. It exhibits large porosity with some fibre pull-out.
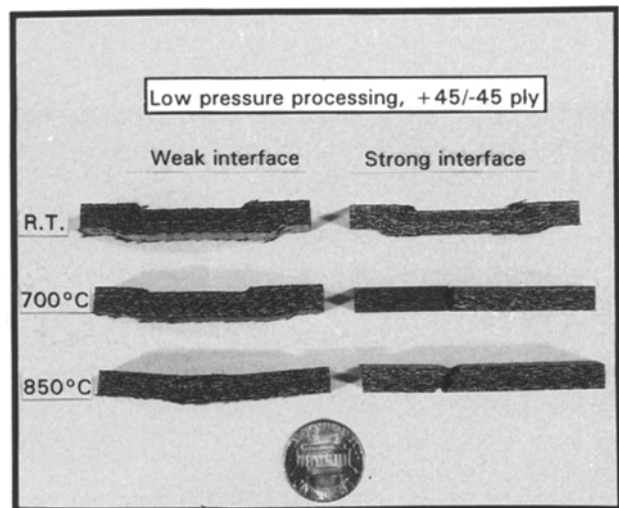
Figure 10 A low magnification photograph of $(+45/−45)_{4s}$-type LPPC tested at different temperatures showing different types of failures under four-point bend loading.

major difference in the failure modes of the $(0/90)_{4s}$ oriented and the $(+45/−45)_{4s}$ oriented composites with the strong fibre/matrix interface is the plane in which failure occurred. In the $(0/90)_{4s}$ orientation failure occurred on a plane at 45° to the loading axis, while in the $(+45/−45)_{4s}$ orientation the failure plane was parallel to the load axis. Fig. 11 shows the flexure strengths of the $(+45/−45)_{4s}$ oriented composites as a function of temperature. At room temperature both the $(0/90)_{4s}$ oriented and the $(+45/−45)_{4s}$ oriented composites with a strong fibre/matrix interface had similar flexure strengths, but at higher temperatures the $(0/90)_{4s}$ orientation had better properties than the $(+45/−45)_{4s}$ orientation. The failure mechanism in the $(+45/−45)_{4s}$ oriented strong interface composite at elevated temperatures was due to fibre breakage with very little pull-out, as shown in Fig. 12. It also shows that there was good bonding between the matrix and the fibres and that the cracks propagated through both matrix and fibres.

The flexure strength of the $(+45/−45)_{4s}$ LPPC with the weak fibre/matrix interface showed a drop as the temperature was increased to 700 °C followed by
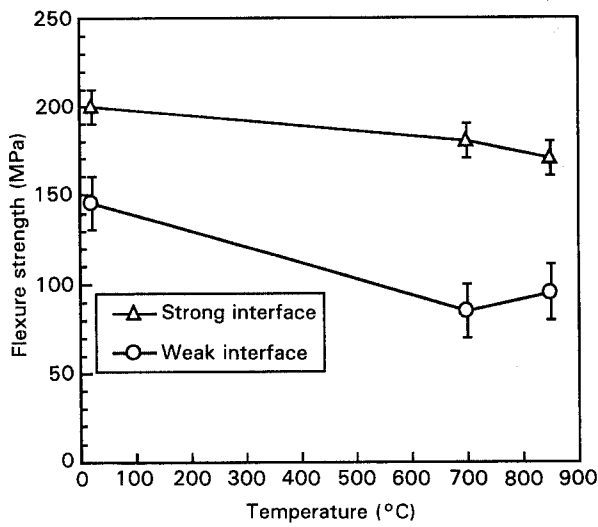
4211

Figure 11 Flexure strengths of low pressure processed $(+45/-45)_{4s}$-type weak and strong interface composites tested at three different temperatures.
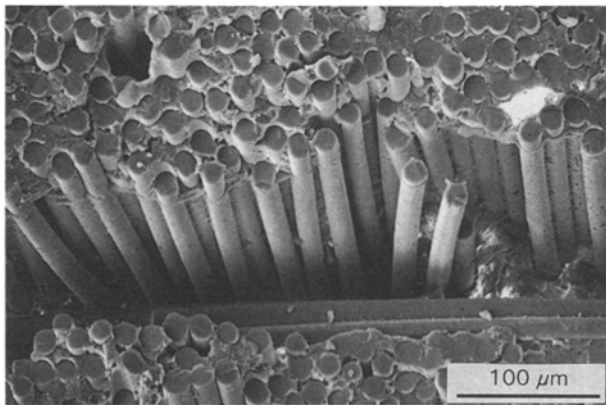

Figure 13 A low magnification photograph of $(0/90)_{4s}$-type HPPC tested at different temperatures showing different types of failures under four-point bend loading.

Figure 12 SEM fractograph of the $(+45/-45)_{4s}$-type LPPC with a strong interface composite tested at 700 °C. It exhibits strong bonding between fibre and matrix material.

Figure 14 Flexure strengths of high pressure processed $(0/90)_{4s}$-type weak and strong interface composites tested at three different temperatures.

an increase at 850 °C. Arguments presented for the $(0/90)_{4s}$ orientation are equally valid here. For the composite with the strong interface there was a monotonic drop in flexure strength with an increase in temperature. As mentioned in the case of the $(0/90)_{4s}$ orientation the primary reasons for the drop in strength in the strong interface composites was due to: (i) degradation of the fibres; (ii) CTE mismatch between the fibres and the matrix.

3.3.4. High pressure processed composites (HPPC)

The porosity content of the composite was significantly reduced due to the additional high pressure applied during various stages of the processing of the composite, as shown in Fig. 1 and Table I. There were some significant differences in the deformation and failure behaviour of the HPPC when compared with the LPPC. As in the case of the LPPC, ply orientation, fibre/matrix interfaces and temperatures of testing were three major variables affecting deformation behaviour.
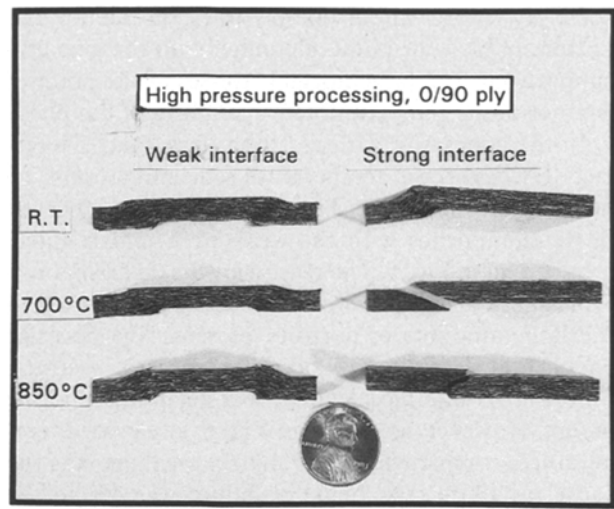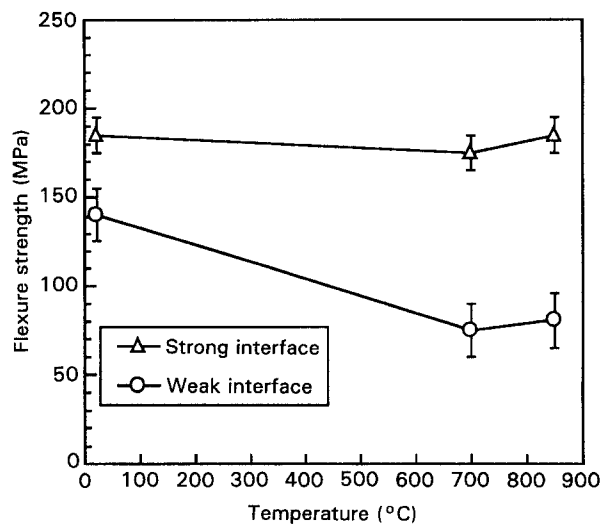
3.3.4.1. $(0/90)_{4s}$ ply orientation in HPPC. The variables used in this analysis included the type of fibre/matrix interface and the temperature of testing. Fig. 13 shows a lower magnification photograph of the different types of failures as a function of temperature. As in the LPPC, the composites with the weak fibre/matrix interfaces failed by a shear induced delamination between the pins of the load span and support span. Fig. 14 shows the flexure strength data for this orientation as a function of temperature and type of fibre/matrix interface. As in the LPPC, the composites with a weak fibre/matrix interface exhibited a greater damage tolerance. A comparison of Fig. 7 and Fig. 14 indicates similar strength levels in the LPPC (25% porosity) and HPPC (10% porosity) for this orientation. This result is rather significant considering the large differences in density and porosity levels. A possible explanation is that within the limits measured, porosity does not play a role in the $(0/90)_{4s}$ orientation.
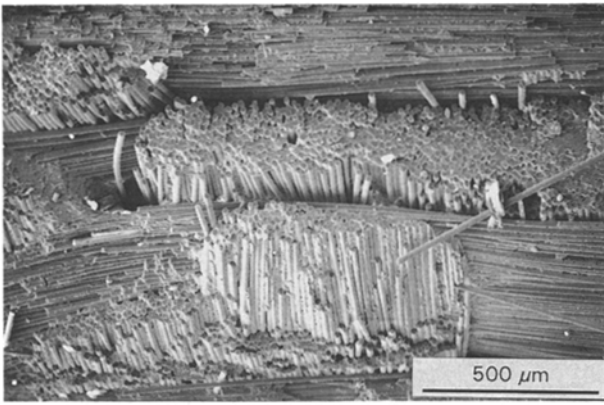
Figure 15 SEM fractograph of the (0/90)₄ₛ-type HPPC with a strong interface tested at 700 °C. It exhibits some fibre pull-out and fibre fracture.
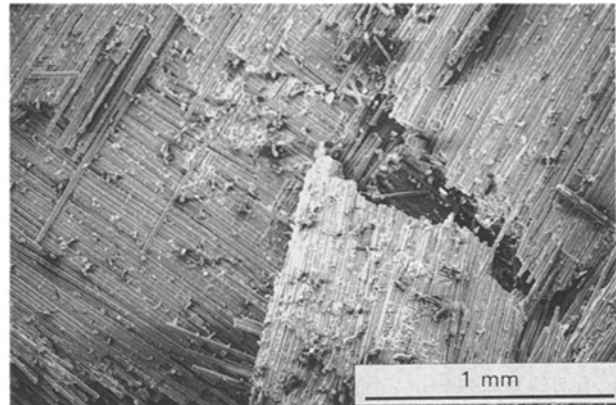

Figure 17 SEM fractograph of the (+45/−45)₄ₛ-type HPPC with a strong interface tested at room temperature. It exhibits a combination of delamination and fibre breakage.
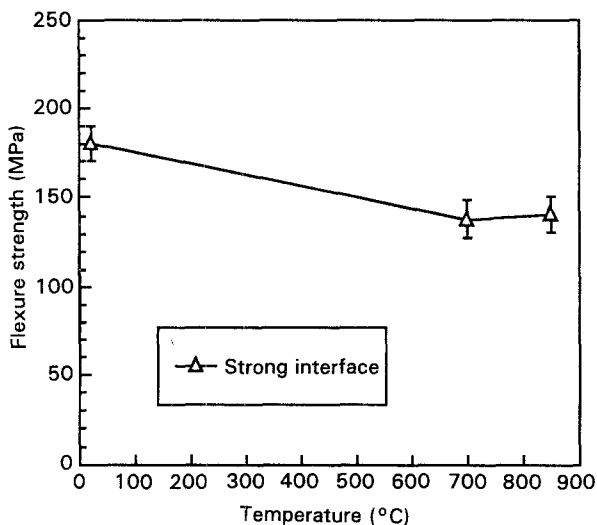

Figure 16 Flexure strengths of high pressure processed (+ 45/ − 45)₄ₛ-type strong interface composites tested at three different temperatures.

Figure 18 SEM fractograph of the (+45/−45)₄ₛ-type HPPC with a strong interface tested at 700 °C. It exhibits a strong bonding between fibres and matrix materials, and cracking across both the fibres and matrix.

The fracture surface of the HPPC with the strong fibre/matrix interface showed little porosity and the failure mechanism was primarily due to fibre and matrix breakage, as shown in Fig. 15.

3.3.4.2. (+45/−45)₄ₛ *ply orientation in HPPC.* HPPC with strong fibre/matrix interfaces were tested. Tests indicated a significant drop in the flexure strength with an increase in temperature, as shown in Fig. 16. A combination of delamination and fibre breakage was observed at room temperature, as shown in Fig. 17. As the temperature was increased a flat fracture surface, which was parallel to the loading axis, was observed, this is similar to the case of the LPPC with a strong fibre/matrix interface. Fig. 18 is a scanning electron micrograph of the composite with a strong interface tested at 700 °C. It clearly shows very good bonding between fibres and matrix material. Very little pull-out was seen at either 700 °C or at 850 °C.

3.3.5. Modulus of elasticity in bending

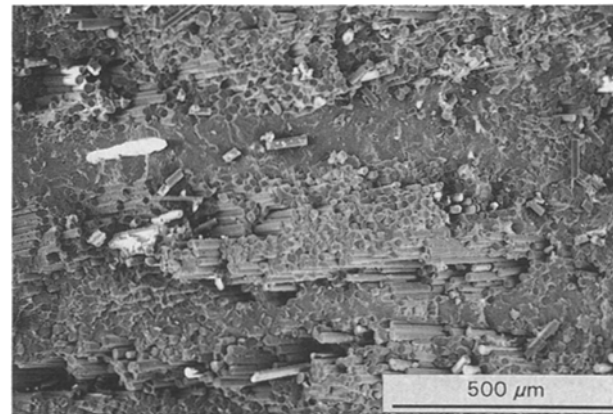The modulus of elasticity in bending was calculated for all the composites from experimental data. In both HPPC and LPPC with strong interfaces, tested at either 700 °C or 850 °C, the modulus of elasticity in bending was 35 GPa for the (0/90)₄ₛ composites and ca. 32.5 GPa for the (45/−45)₄ₛ composites. The weak interface composites did not exhibit any Hookean region. The secant modulus of elasticity was calculated and is ca. 24.1 GPa for the (0/90)₄ₛ-type composites and 22.3 GPa for the (45/−45)₄ₛ-type composites at all temperatures. The strong interface composites tested at room temperature did not show any Hookean region and the secant modulus of rigidity was ca. 29.5 GPa for the (0/90)₄ₛ-type and 27 GPa for the (45/−45)₄ₛ-type composites. The lower values of the modulus for the (45/−45)₄ₛ-type lay-up is a consequence of the orientation of the fibres.

4. Discussion

Oxidation tests indicated that there was little or no change in weight even after 6000 min at 850 °C in an atmosphere of air. The elemental X-ray dot mapping technique used to determine the location of P, Si and Al indicated no movement of the atoms up to a magnification of × 2000. However, this does not preclude the presence of fibre/matrix interaction at

4213

the microscale which can lead to property degradation.

Due to the various variables involved in the processing, the flexure properties are a synergistic interaction of several of these variables. However, it is possible to isolate some of these variables which include (a) the type of fibre/matrix interaction, (b) orientation of the plies and (c) temperature of testing to a greater extent and porosity content to a lesser extent.

The most prominent factor that affected both the mechanism of failure and the flexure strength was the nature of the fibre/matrix interface. Carbon coated and uncoated Nicalon™ fibres were used to produce weak and strong interfaces, respectively. As a rule, the presence of a weak interface promoted fibre/matrix sliding and produced a more damage tolerant composite, with failure occurring by shear dominated delamination with little fibre breakage. On the other hand, fibres that did not have a coating were susceptible to attack from the matrix during processing and formed a strong interface. These composites, as a rule, failed by complete fibre and matrix breakage at elevated temperatures. The strong interface composites, in general, had flexure strengths 10–20% greater than the weak interface for comparable porosity contents and orientation.

The orientation of the plies did not play a role in either the mechanism of failure or the strength of the weak interface composites, where failure occurred by delamination rather than fibre breakage. The simple two-dimensional finite element model presented for a monolithic material, tested under four-point bend loading, indicated shear stresses with a magnitude of as high as 45 times the applied normal stress existing between the support and load points. As delamination occurred due to fibre sliding and interface decohesion, orientation was not an important factor. On the other hand, the failure mode of the strong interface composites was affected by the orientation of the plies. At higher temperatures the failure plane was parallel to the load axis in the $(+45/-45)_{4s}$ orientation, whereas the $(0/90)_{4s}$ composite exhibited a fracture plane at 45° to the load axis. This result is consistent with the general observation of strong interface, polymer-based composites. As a rule, $(0/90)_{4s}$ orientation exhibited higher strength than the $(+45/-45)_{4s}$ oriented composites when porosity contents and testing temperatures were kept constant. This is because the $(0/90)_{4s}$ composites exhibited ca. 50% reinforcement efficiency in the direction of testing, whereas in the $(+45/-45)_{4s}$ composites the efficiency of reinforcement was ca. 40%. Fibre breakage was observed at the point of contact with the pins, which extended no more than one or two plies. Two-dimensional finite element simulations for point loads indicated a significant increase in σ_{yy} stresses at the point of contact which decreased rapidly away from the surface.

Temperature played a significant role in determining the type of failure, as well as flexure strength. In the composites with a weak fibre/matrix interface, increasing the temperature from room temperature to 850 °C did not change the mode of failure, which

remained shear dominated delamination. However, after an initial drop in strength at 700 °C there was an increase in strength at 850 °C in all orientations and porosity contents. This indicated that up to 700 °C, there was almost no fibre/matrix interaction and the drop in strength was due to easier sliding of the fibres. At 850 °C, it appeared that the fibre/matrix reactions were initiated at the microscale levels, forming a stronger bond and an increased strength. This increase in strength placed these composites with a strength level below that of the strong interface composites with similar orientations and temperatures of testing. Composites with a strong interface exhibited a change in the mode of fracture as the temperature was increased. At room temperature the HPPC exhibited a delamination-type failure, while at higher temperature a clean break with fibre and matrix fracture occurred. LPPC with strong interfaces exhibited an increase in strength from room temperature to 700 °C followed by a drop at 850 °C. The initial increase can be attributed to a change in the mode of failure while the final drop in flexure strength was due to two possible causes; (a) degradation of the fibre/matrix interface and/or fibres and (b) increased residual stresses due to the higher temperature.

The LPPC had a porosity of 25% while the HPPC had a porosity of 10%. Within these limits, porosity did not play a major role compared to the effects of fibre/matrix interface, temperature and orientation.

5. Conclusions

Based on the present study, the following conclusions can be drawn on the thermal and mechanical behaviour of those composites.

1. The small weight change exhibited by the composites on exposure to air for 6000 min at 850 °C indicate stable composites and no carbon sublimation.

2. Changing the porosity content from 10 to 25% played a minor role in influencing the flexure properties compared to other factors, like temperature, orientation and type of interface.

3. In both the LPPC and HPPC composites, with increasing temperature the flexure strength remained almost constant for the $(0/90)_{4s}$ oriented composite with the strong fibre/matrix interface. However, there was a drop in the flexure strength for the $(+45/-45)_{4s}$ oriented composite with a strong fibre/matrix interface.

4. In all composites with a weak fibre/matrix interface there was a drop in flexure strength at 700 °C followed by an increase in flexure strength at 850 °C. However, the strength never approached that of the strong fibre/matrix interface composites under similar conditions.

5. A deformation/delamination-type failure between the pins of the load span and the support span was observed for all the composites with a weak fibre/matrix interface irrespective of temperature and orientation of testing.

6. Composites with either the $(0/90)_{4s}$ orientation or the $(+45/-45)_{4s}$ orientation with strong fibre/

matrix interfaces showed a clear failure into two piece for both HPPC and LPPC when tested at either 700 or 850 °C. Little or no fibre pull-out was seen. However, at room temperature the LPPC with a strong fibre/matrix interface exhibited a deformation/delamination-type of failure.

Acknowledgements

References

1. M. K. FREBER and V. J. TENNERY, "Engineering materials handbook", Vol 4 (ASM) p. 959.
2. W. R. CANON and T. G. LANGDON, J. Mater. Sci. **23** (1988) 1.
3. L. EWART and S. SURESH, J. Mater. Sci. **22** (1987) 1173.
4. M. RÜHLE and A. G. EVANS, Progr. Mater. Sci. **33** (1989) 85.
5. R. O. RITCHIE, in Proceedings of the 5th International Conference of Mechanical Behaviour of Materials, Edited by M. G. Yan, S. H. Zhang and Z. M. Zheng (Pergamon, Oxford, 1988).
6. A. G. EVANS, Phil. Mag. **26** (1972) 1327.
7. J. W. HUTCHINSON, Acta Metall. **35** (1987) 1605.
8. A. G. EVANS and K. T. FABER, J. Amer. Ceram. Soc. **67** (1984) 255.
9. F. F. LANGE, Phil. Mag. **22** (1970) 983.
10. J. R. BROCKENBROUGH and S. SURESH, Acta. Metall. **38** (1990) 55.
11. D. M. ROY, Science **635** (1987) 651.
12. R. E. STEINKE, M. R. SILSBEE, D. K. AGRAWAL, R. ROY and D. M. ROY, Cement Concrete Res. **21** (1991) 66.
13. Y. MING CHIANG, J. S. HAGGERTY, R. P. MESSNER and C. DEMETRY, Ceram. Bull. **68** (1989) 420.
14. T. C. SIMONTON, R. ROY, S. KOMERANENI and E. BREVAL, J. Mater. Res. **1** (1986) 667.
15. R. A. MARRA, D. J. BRAY, D. J. MOESLEIN and M. V. VANCE, "Aluminium phosphate bonded ceramics composites", ALCOA Technical Report (1991).
16. C. ZWEBEN and J. C. NORMAN, SAMPE Q. July (1976) 1.
17. T. ISHIKAWA and T. W. CHOU, J. Mater. Sci. **17** (1982) 3211.
18. T. ISHIKAWA and T. W. CHOU, J. Mater. Sci. **18** (1983) 2260.
19. L. W. CHANG, S. S. YAU and T. W. CHOU, Composites **18** (1987) 233.
20. F. J. GONZALEZ and J. W. HALLORAN, Amer. Ceram. Soc. Bull. **59** (1980) 727.
21. R. M. JONES, "Mechanics of composites materials" (Scripta, Washington DC., 1975).
22. T. ISHIKAWA and T. W. CHOU, J. Mater Sci. **17** (1982) 3217.